Journal of Multidisciplinary Engineering Science and Technology (JMEST)
ISSN: 2458-9403
Vol. 8 Issue 1, January - 2021

Template-Based Fabrication of Vertically Aligned Carbon Nanotube Arrays

Masoud Golshadi[1], Lan Nguyen[2], Ian M. Dickerson[3], and Michael G. Schrlau[4*]

[1]Department of Microsystems Engineering, Rochester Institute of Technology, Rochester, NY, USA
[2]Department of Chemical and Biochemical Engineering, Brown University, Providence, RI, USA
[3]Department of Neuroscience, University of Rochester Medical Center, Rochester, NY, USA
[4]Department of Mechanical Engineering, Rochester Institute of Technology, Rochester, NY, USA
*Corresponding Author: mgseme@rit.edu

***Abstract*—Vertical arrays of nanowires and nanotubes have recently been used in an increasing number of applications. These applications almost invariably rely on the physical features of these nanoelements, necessitating a better control over their geometrical properties to improve their performance. Here, we report the manufacturing process of vertically aligned, hollow carbon nanotube (CNT) arrays of different tube diameters, spacing, and length as needed for their intended application. A template-based manufacturing method was employed to form CNTs inside the pores of commercially available anodized aluminum oxide membranes using chemical vapor deposition. After removing the carbon layer from the surface of the membrane with oxygen plasma, the membrane surface was selectively removed by either reactive ion etching, wet chemical etching, or a combination of ion milling and wet etching to expose the CNTs embedded in the membrane. The results show that to reach longer individually addressable exposed CNTs, dry etching processes like RIE are more promising. The work provides a scalable and reliable manufacturing recipe for a CNT-based array device that can be used for various sensing and also biomedical applications.**

Keywords: Carbon Nanotube, Carbon Nanotube Arrays, Template-Based Manufacturing, Anodized Aluminum Oxide, Chemical Vapor Deposition, Reactive Ion Etching, Wet Chemical Etching

I. INTRODUCTION

In recent years, growing interest towards creating novel nanoscale devices for elucidating cellular behavior has enabled significant advances in biomedical and clinical applications [1-3]. Of particular interest are vertically-aligned arrays of nanostructures for interfacing with living cells and tissues [4, 5]. Nanoarray devices have been employed to measure forces of adherent cells [6] and utilized as various biomolecular and chemical sensors [7, 8]. One of the unique features of nanoarrays is their ability to access the cell's cytosol, resulting in broad biomedical applications [9-11]. Such applications include utilizing nanoarrays to observe intracellular biochemical activity [12], measure intracellular and extracellular signals [13], and deliver drugs, nanoparticles and biomolecules, such as quantum dots, nucleic acids and proteins, directly into cells [14-18].

The ever-growing demand for vertically aligned nanostructured arrays in biomedical applications necessitates the ability to control the geometrical features of the nanostructures, such as length, diameter, orientation and packing density, since these features play a crucial role in the performance of the arrays. As biological and chemical sensors, the sensitivity of array electrode-based sensors can be increased by exposing more of the nanostructure in the array thus increasing the available surface area for detection [19, 20]. In applications requiring cell-array interfacing, such as cell proliferation, differentiation, adhesion and migration [21, 22], *in situ* study of intracellular molecular processes [12] and efficient intracellular delivery [17, 23, 24], geometrical features influence how well the nanostructures interact with the cell membrane. Studies have found that transfection efficiency and intracellular access depend on the length of the nanostructures in the array [17, 25]. Optimizing the length and spacing of arrayed nanostructures promotes cell adhesion onto its surface and enables the nanostructures to penetrate the membrane without causing detrimental effects [11].

In our own work on carbon nanotube (CNT) array-based gene transfection, cells adhered well to tightly-packed arrays of short lengths of exposed CNTs, which promoted highly efficient delivery of macromolecules, quantum dots and plasmid DNA into tens of thousands of adherent cells simultaneously [14]. As shown in Fig. 1, these CNT-based array devices are manufactured using a three-step process: First, an anodized aluminum oxide (AAO) porous membrane is selected to serve as a sacrificial template. Next, CNTs are formed inside the AAO membrane using established template-based chemical vapor deposition (CVD) processes [26]. Finally, carbon is removed from one side of the AAO membrane using oxygen plasma and then, the tips of the CNTs embedded in the AAO membrane are exposed using selective etching techniques. The

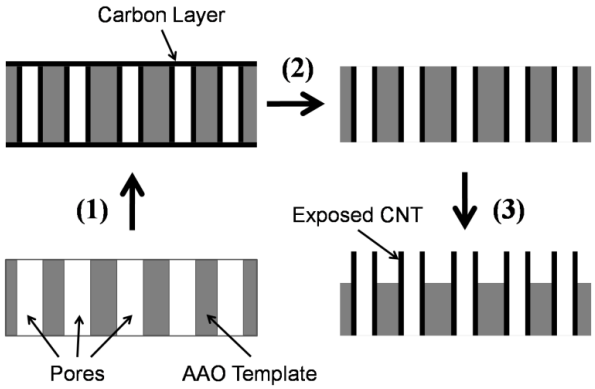

Fig. 1: Schematic illustration of the device fabrication procedure. Fabrication process showing (1) carbon deposition by chemical vapor deposition, (2) removing the amorphous carbon layer by oxygen plasma, (3) exposing the CNT tips by either reactive ion etching, wet chemical etching, or a combination of ion milling and wet etching process.

resultant CNT-based array device consists of millions of vertically aligned, hollow and conductive CNTs protruding from the surface of a sacrificial membrane. The porous AAO membrane dictates the outer diameter and spacing between the CNTs, whereas the selective etching process controls the length of the exposed CNT tip. Dozens of these array devices can be manufactured without assembly in a single run, making the process amenable for further scale-up.

Here, we report the development and fabrication of the CNT-based array device and describe several approaches to expose and control the length of the CNTs protruding from the device surface. Commercially available AAO membranes of varying pore sizes and interpore distances were utilized as the sacrificial template to produce CNT-based array devices. The CNT tips were exposed using either reactive ion etching (RIE), wet chemical etching, or a combination of ion milling and wet etching. The effect of etching process and associated process parameters on the exposed length of the CNTs are discussed and compared. Ultimately, this report serves as a guide for manufacturing vertically aligned, hollow CNT arrays of different tube diameters, spacing, and length as needed for their intended application. Moreover, our results have identified parameters that influence cell attachment, proliferation and gene transfer efficiency. These parameters have been validated for immortalized cell lines [14], and have potential for future studies to facilitate gene transfer into cells not amenable to standard transfection techniques, such as stem cells, primary neurons, and immune cells.

II. Experimental Methods

A. Template Preparation

Commercially available AAO membranes were used as a sacrificial template for carbon deposition. AAO membranes with the following nominal pore diameters were utilized: 100 nm (Synkera UniKera, Cat. No.: SM-100-50-13, nominal pore diameter: 100±10 nm, nominal thickness: 50±1 µm), 150 nm (Synkera UniKera, Cat. No.: SM-150-50-13, nominal pore diameter: 150±10 nm, nominal thickness: 50±1 µm), and 200 nm (Whatman Anodisc 13, Cat. No.: 6809-7023, nominal pore diameter: 200 nm, nominal thickness: 60 µm). To prevent curling of the membranes during the CVD process [26, 27], membranes were first annealed 30 °C above synthesis temperature for 4 hours between two quartz plates.

B. Carbon Deposition

Carbon film was deposited inside the pores of AAO templates to form CNTs using previously reported methods [26]. In brief, AAO membranes were placed upright in a custom quartz boat and positioned in the middle of a three-stage tube furnace (Carbolite, TZF17/600, inner tube diameter: 7 cm, tube length: 152 cm). The reactor temperature was slowly increased to 700 °C under 100 sccm of argon gas flow. After temperature stabilization, 60 sccm of 30/70 (vol%/vol%) ethylene/helium gas was flown through the reactor tube for 5 hours to deposit carbon film on all surfaces of the AAO membrane. The furnace was then slowly ramped down to room temperature under 100 sccm of argon flow. The effect of synthesis parameters on carbon deposition and CNT formation was reported in detail elsewhere [26].

C. CNT Tip Exposure

Deposited carbon layer over the AAO template after CVD was removed by oxygen plasma at 250 W, 300 mTorr for 3.75 minutes under 100 sccm of oxygen flow (LAM 490) before etching process.

1) Reactive Ion Etching

Reactive Ion Etching (RIE, LAM 4600 Etcher) was employed to selectively etch AAO templates in order to partially expose the tips of embedded CNTs. Etching occurred using a combination of boron trichloride (BCl_3) and chlorine (Cl_2) gases (100 sccm combined flow) under constant chamber pressure (150 mTorr) at different RF power (200-400 W) for various durations (approximately 2-5.5 hours).

The effect of etching time, RF power and gas combination on CNT exposure length were studied in an orthogonal manor; in each set of experiments, one parameter was changed while the others remained unchanged. Orthogonal experiments were conducted for 100%/0%, 75%/25%, 50%/50%, 257%/75% and 0%/100% of BCl_3 and Cl_2 gases, respectively, RF power of 200, 300 and 400 W, and up to 315 minutes of etching time at 150 mTorr chamber pressure.

2) Wet Chemical Etching

Wet chemical etching using various acids and bases was employed to partially expose the CNTs. To this end, 0.5 M aqueous solution of sulfuric acid (H_2SO_4), hydrochloric acid (HCl), phosphoric acid (H_3PO_4), acetic acid (CH_3COOH), formic acid (HCOOH) and also sodium hydroxide (NaOH) and potassium hydroxide (KOH) were utilized to dissolve the template at room temperature for 15 minutes. The samples were then rinsed for 15 minutes with distilled water and dried overnight before imaging.

The effect of etching time on CNT exposed length was studied for all three membranes. Carbon deposited AAO membranes were submerged in 1 M aqueous sodium hydroxide solution for 4, 6, 8, 10, 12, 14 and 18 minutes at room temperature. The samples were then rinsed for 15 minutes with distilled water and dried overnight before imaging. The exposed length of the CNTs was measured using SEM micrograph.

3) Ion Milling and Wet Chemical Etching

The CNTs were exposed by a combination of ion milling and wet etching processes. After CVD, the template surface was etched by ion milling at 800 V, 45-degree argon ion shower angle for 2 hours (AJA Ion Mill). Membranes were then etched in 1 M aqueous NaOH solution for 9 and 15 minutes to expose the tips. Samples were then rinsed for 15 minutes with distilled water and dried overnight before imaging.

D. Characterization

The exposed length of CNT tips, the surface morphology and the integrity of individual CNTs after each exposing process were examined and measured using scanning electron microscopy (SEM, Zeiss Auriga; 20 kV acceleration voltage). The samples were characterized without sputter coating.

III. Results and Discussion

A. Commercially Available AAO Membranes

To provide a reproducible and cost-effective fabrication process for a device that can be utilized in a variety of biological and biomedical applications, commercially available AAO membranes were used.

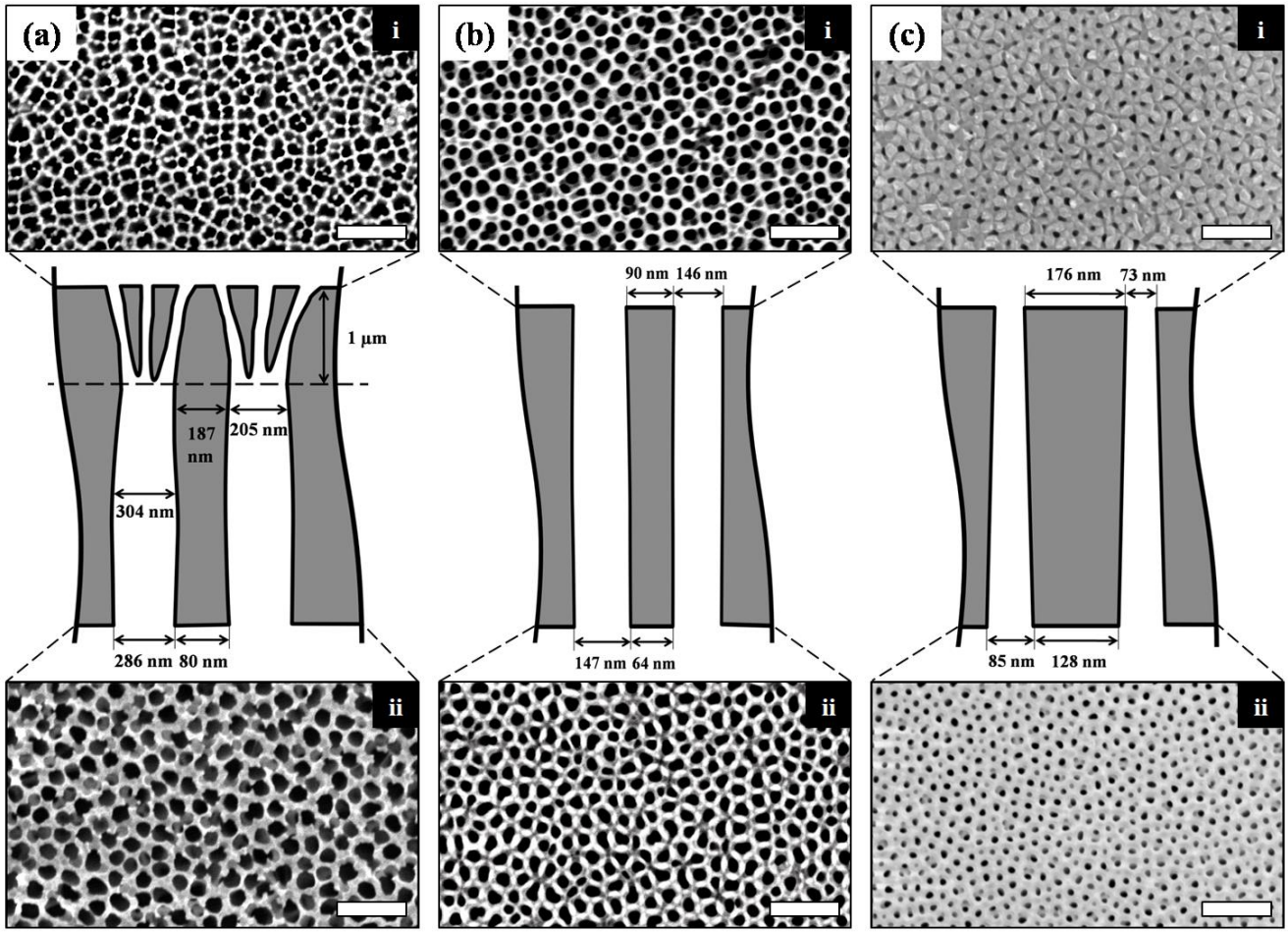

Fig. 2: AAO membrane pore structure. SEM micrographs of both surfaces along with the schematics of the pore structure for (a) Whatman 200 nm AAO membrane, (b) Synkera 150 nm AAO membrane, and (c) Synkera 100 nm AAO membrane. (Scale bars: 1 µm)

Since the pore diameter of the AAO membrane dictates the outer diameter of resultant CNTs, pore diameters on both sides of the membrane were characterized by SEM. Three different AAO templates from two different manufacturers were investigated: Whatman AAO membranes with 200 nm nominal pore diameter and Synkera AAO membranes with 100 nm and 150 nm nominal pore diameter.

Fig. 2 shows the SEM micrographs of the surfaces of these membranes along with a schematic of their pore structure. The average pore diameter and interpore distance (side-to-side) were found to be, respectively, as follows: 205±42 nm and 187±36 nm on one side (Fig. 2(a-i)), 286±48 nm and 80±24 nm on the other side (Fig. 2(a-ii)) for Whatman 200 nm templates (n=480); 146±29 nm and 90±14 nm on one side (Fig. 2(b-i)), 147±20 nm and 64±19 nm on the other side (Fig. 2(b-ii)) for Synkera 150 nm templates

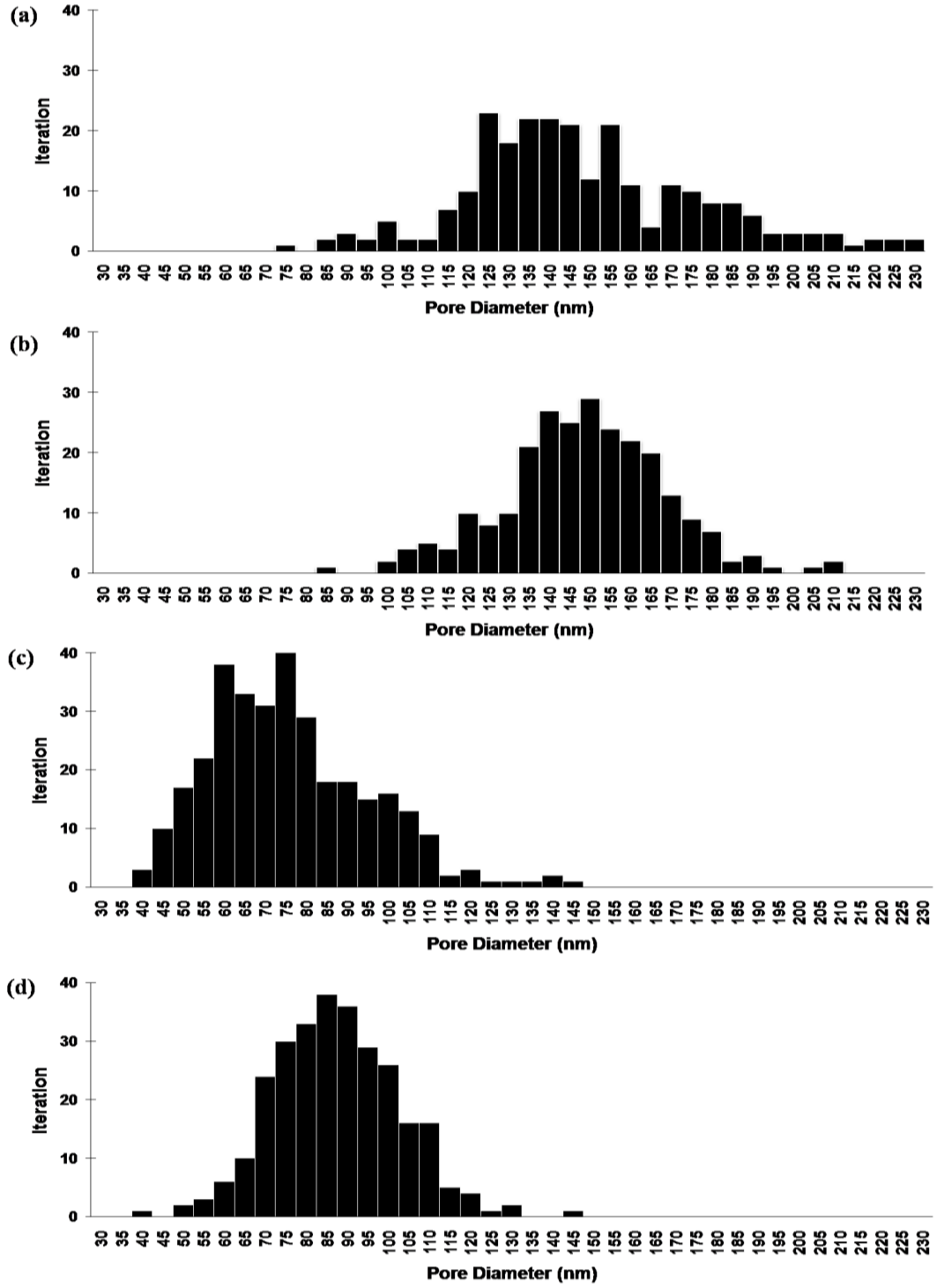

Figure 3. Histograms of the template pore diameter measurement using SEM micrographs of the two AAO surfaces for Synkera 150 nm and 100 nm membranes. The average pore diameter was found to be 146±29 nm on one side (Fig. 3(a)) and 147±20 nm on the other side (Fig. 3(b)) for Synkera 150 nm templates (n=250), 73±19 nm on one side (Fig. 3(c)) and 85±17 nm on the other side (Fig. 3(d)) for Synkera 100 nm templates (n=330).

Table 1: Overview of Experiments and Measurements

Type of the Process	Parameter	AAO Template	Etching Time (min)	RF Power (W)	Gas Combination (BCl_3% / Cl_2%)	Gas Flow Rate (sccm)	Chemical Etchant	CNT Exposed Length ± Standard Deviation (nm)
Reactive Ion Etching	Effect of the Etching Time	Whatman 200 nm	135	400	100% / 0%	100	NA	152 ± 77
			150					113 ± 26
			180					176 ± 34
			195					177 ± 44
			225					293 ± 97
			270					314 ± 115
			315					389 ± 169
		Synkera 150 nm	135	400	100% / 0%	100	NA	48 ± 26
			195					81 ± 20
			225					186 ± 52
	Effect of the RF Power	Whatman 200 nm	150	200	100% / 0%	100	NA	0
				300				0
				400				113 ± 26
	Effect of the Gas Mixture	Whatman 200 nm	150	400	0% / 100%	100	NA	0
					25% / 75%			0
					50% / 50%			0
					75% / 25%			0
					100% / 0%			113 ± 26
Wet Chemical Etching	Effect of the Etching Time	Whatman 200 nm	4	NA	NA	NA	1M NaOH	0
			8					0
			10					42 ± 12
			14					153 ± 22
			16					208 ± 46
		Synkera 150 nm	4	NA	NA	NA	1M NaOH	0
			6					0
			8					73 ± 21
			10					196 ± 32
			12					238 ± 89
			14					645 ± 123
		Synkera 100 nm	4	NA	NA	NA	1M NaOH	0
			6					0
			8					43 ± 15
			10					85 ± 33
			12					108 ± 25
			14					118 ± 44
			18					167 ± 56
Wet Chemical Etching after Ion Milling	Effect of the Etching Time	Whatman 200 nm	9	NA	NA	NA	1M NaOH	100 ± 27
			15					183 ± 48

(n=250); 73±19 nm and 176±39 nm on one side (Fig. 2(c-i)) and 85±17 nm and 128±31 nm on the other side (Fig. 2(c-ii)) for Synkera 100 nm templates (n=330). Fig. 3 shows the detailed histograms of the measured pore diameter for Synkera; the detailed analysis of pore diameter for Whatman membranes has been reported elsewhere [26].

The AAO membrane pore density was found to be $11.6x10^8$, $22.1x10^8$, and $15.3x10^8$ pores per centimeter square for Whatman 200 nm, Synkera 150 nm and Synkera 100 membranes, respectively. As the results show, the pore structure is more uniform and cylindrical for Synkera membranes with a shorter interpore distance, while the Whatman membranes have a barrel shaped pore formation and longer interpore spacing. Moreover, there is almost a 1 µm deep branch-shaped structure on one side of the Whatman AAO membranes compared to Synkera, which is due to the difference between the fabrication processes of the two manufacturers. Although Synkera membranes provided more uniform pore diameters and spacing without the branched structure, Whatman membranes facilitate the production of CNT array devices due to their lower cost (6X less than Synkera) and larger interpore spacing (mitigates lateral adhesion between exposed CNTs [28, 29]).

B. CNT Tip Exposure

The AAO membrane was selectively removed to expose the tips of CNTs embedded inside the pores of the sacrificial template. Three selective etching approaches were investigated: (1) RIE, (2) wet etching, and (3) a combination of ion milling and wet etching. Table 1 summarizes the experiments conducted to expose the CNT tips, the associated parameter settings and the resultant average exposed length of the CNTs.

1) Reactive Ion Etching

There are several parameters that can affect the etch rate of AAO membranes using RIE, including gas combination, gas flow rate, chamber pressure, RF power and etching time. Among these parameters, etching time, RF power and gas combination were identified in preliminary experiments as the most influential on AAO etch rate and were therefore chosen to study how they affected CNT exposure.

The other settings were set based on the limitations of the equipment and preliminary experiments. For the baseline RIE process (400 W, 100% BCl_3 at 100 sccm, 150 mTorr), the exposed CNT length was measured as a function of etching time for two different membranes, as shown in Fig. 4. The results show that for Whatman AAO (200 nm pore diameter), CNTs are exposed at lengths of 152±77 nm, 113±26 nm, 176±34 nm,

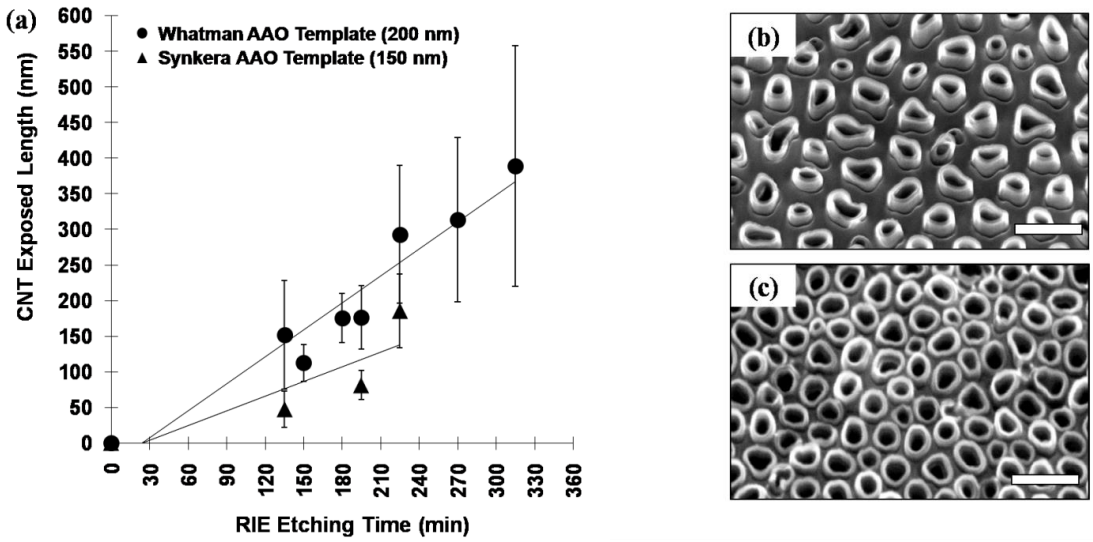

Fig. 4: Effect of RIE etching time on CNT exposure. (a) CNT exposed length as a function of RIE etching time for Whatman (200 nm pore diameter, solid circle) and Synkera (150 nm pore diameter, solid triangle). SEM micrographs of embedded exposed CNTs after 195 minutes of etching under 100 sccm of 100% BCl_3 at 400 W of RF power and 150 mTorr for (b) Whatman and (c) Synkera AAO templates. (Scale bars: 500 nm)

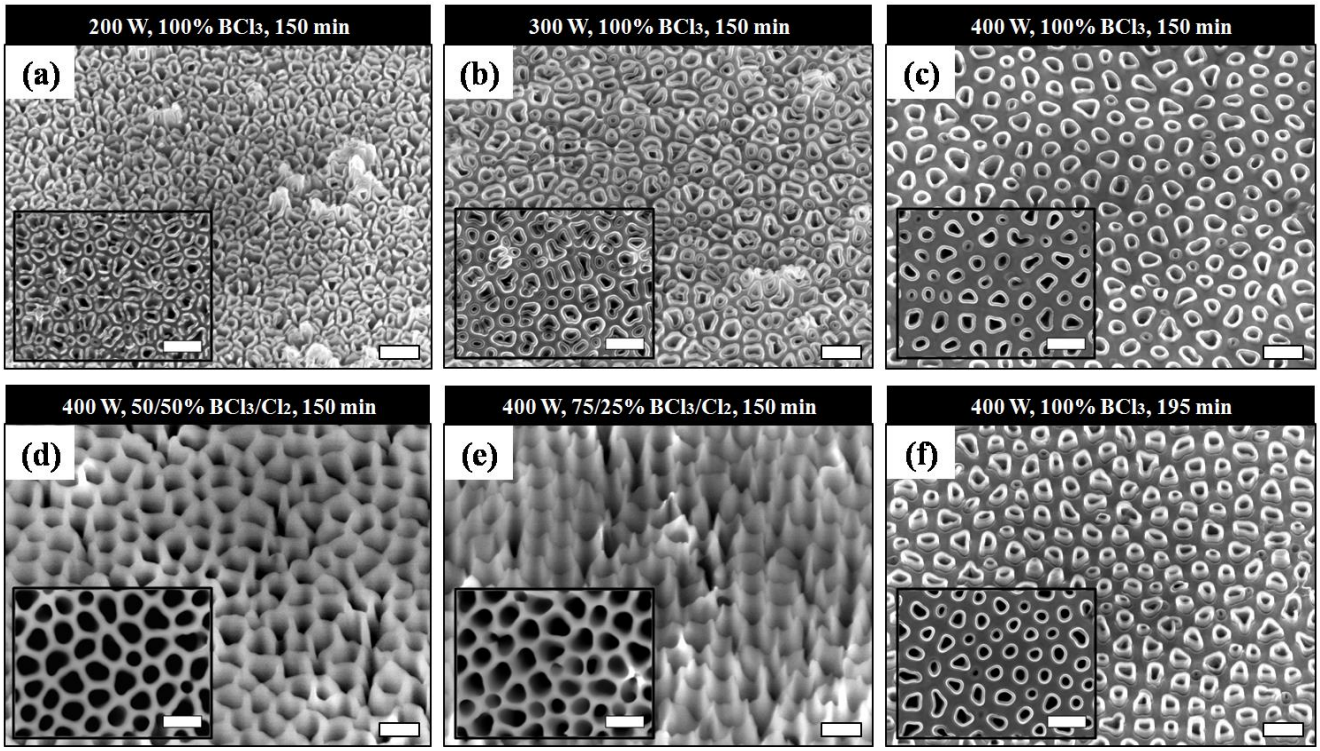

Fig. 5: SEM micrographs of CNT embedded Whatman AAO membranes at 35° tilt, showing the effect of RF power, gas mixture and etching time on CNT exposure after RIE. AAO membranes etched under 100 sccm of 100% BCl_3 at (a) 200 W, (b) 300 W and (c) 400 W of RF power and 150 mTorr for 150 minutes and (f) 195 minutes. Also, AAO membranes etched for 150 minutes by adding (d) 50% and (e) 25% of Cl_2 gas to the mixture with total flow rate of 100 sccm, at 400 W of RF power and 150 mTorr. Insets: top view SEM micrographs of each parameter setting. (Scale bars: 500 nm)

177±44 nm, 293±97 nm, 314±115 nm and 389±169 nm from the AAO surface after 135, 150, 180, 195, 225, 270 and 315 minutes of RIE, respectively. For Synkera AAO (150 nm pore diameter), CNTs were exposed at lengths of 48±26 nm, 81±20 nm and 186±52 nm after 135, 195 and 225 minutes of RIE, respectively. For both membranes, CNT exposure length trended approximately linear as a function of time. However, the lower etch rate of the Synkera membrane suggests a more resistant crystalline structure to RIE etching due to their manufacturing process. For both membranes, the measured standard deviation increased as etching time increased, suggesting a rougher CNT tip surface at longer etching times. This could be due to the nature of the RIE process in which a combination of physical and chemical etching reduces the selectivity of the results. Therefore, the CNTs will be etched but at a slower rate compared to aluminum oxide and the longer they are exposed to the plasma, the less uniform they become.

The effect of RF power on the exposure of the CNT tips was also investigated. To this end, CNT-embedded Whatman AAO templates were etched at 200, 300 and 400 W under 100 sccm of 100% BCl_3 gas flow at 150 mTorr for 150 minutes. As shown in Fig. 5, although increasing the RF power increases the AAO etch rate, which matches our expectation and also other studies [30, 31], no exposed CNTs can be measured at 200 and 300 W (Fig. 5(a, b)). However, CNTs are exposed 113±26 nm from the AAO surface at 400 W after 150 minutes (Fig. 5(c)). Note that the variation of CNT packing density in Fig. 5(a-c) is due to the existence of the branch-shaped structure of the pores on the one side of the Whatman AAO templates (Fig. 2(a-i)) which is completely etched away after 150 minutes of RIE at 400 W.

Combining BCl_3 and Cl_2 gases have been reported to etch aluminum oxide [30, 32-34]. Therefore, the effect of gas mixture on the CNT exposed length was studied. The SEM micrographs of the CNT embedded AAO membranes after 150 minutes of RIE are also presented in Fig. 5. The membranes were etched with 50%/50% and 75%/25% of BCl_3/Cl_2 gases with total gas flow rate of 100 sccm at 400 W and 150 mTorr of chamber pressure (data not shown for higher percentage of chlorine gas). Although introduction of chlorine gas to

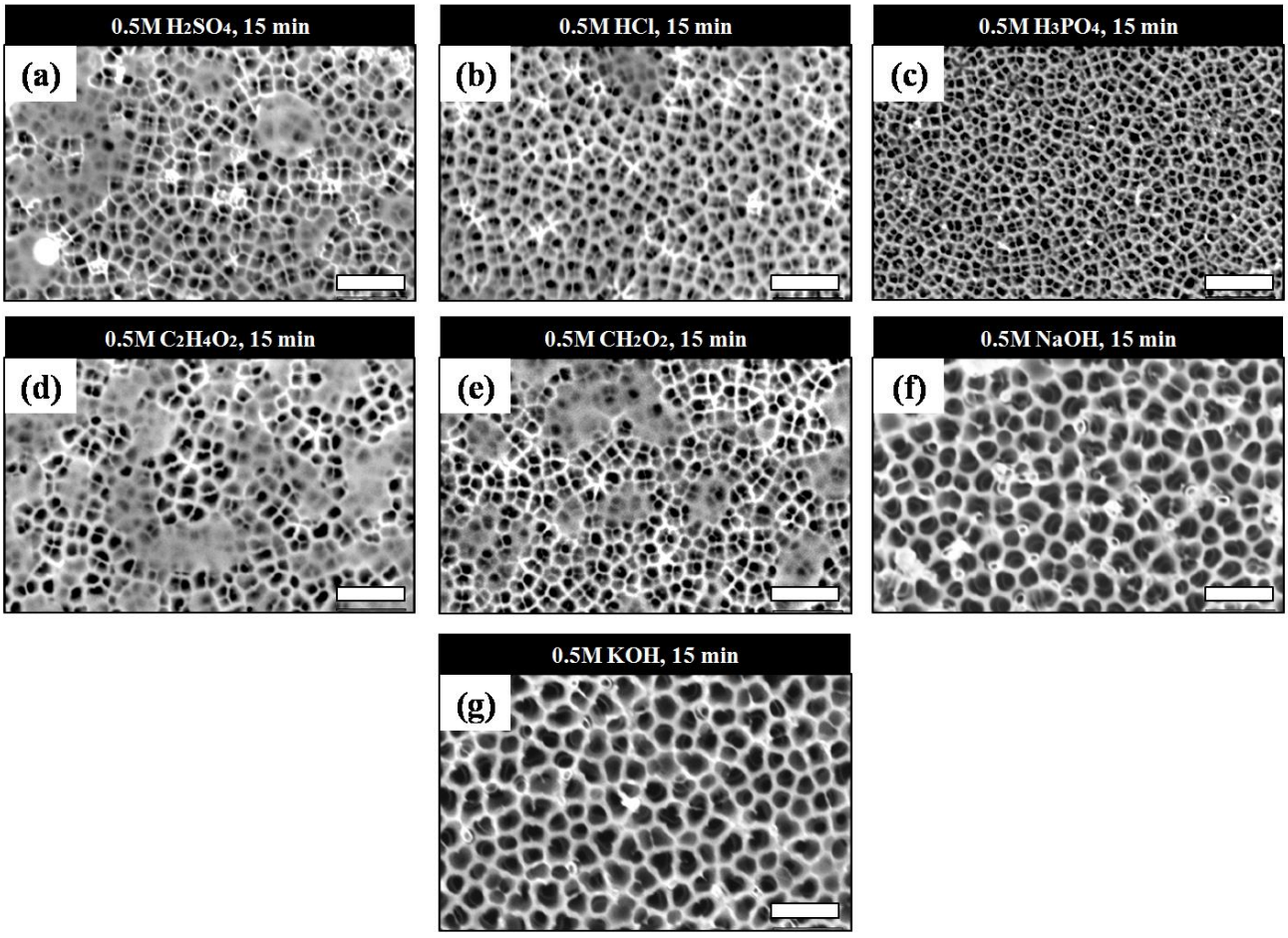

Fig. 6: Effect of wet etchant type on CNT exposure. SEM micrographs of CNT embedded Whatman AAO membranes after 15 minutes of etching in 0.5 M aqueous solution of (a) sulfuric acid, (b) hydrochloric acid, (c) phosphoric acid, (d) acetic acid, (e) formic acid, (f) sodium hydroxide and (g) potassium hydroxide at room temperature. (Scale bars: 1 µm)

the plasma can increase the AAO etch rate [30, 35], the results show that it also increases the carbon etch rate, such that the CNT tip exposure cannot be achieved (Fig. 5(d, e)). Therefore, to partially remove the AAO templates, 100% BCl_3 gas at 100 sccm of flow rate and 400 W of power was selected.

2) Wet Chemical Etching

To selectively remove the AAO templates and expose the CNT tips, wet etching processes were

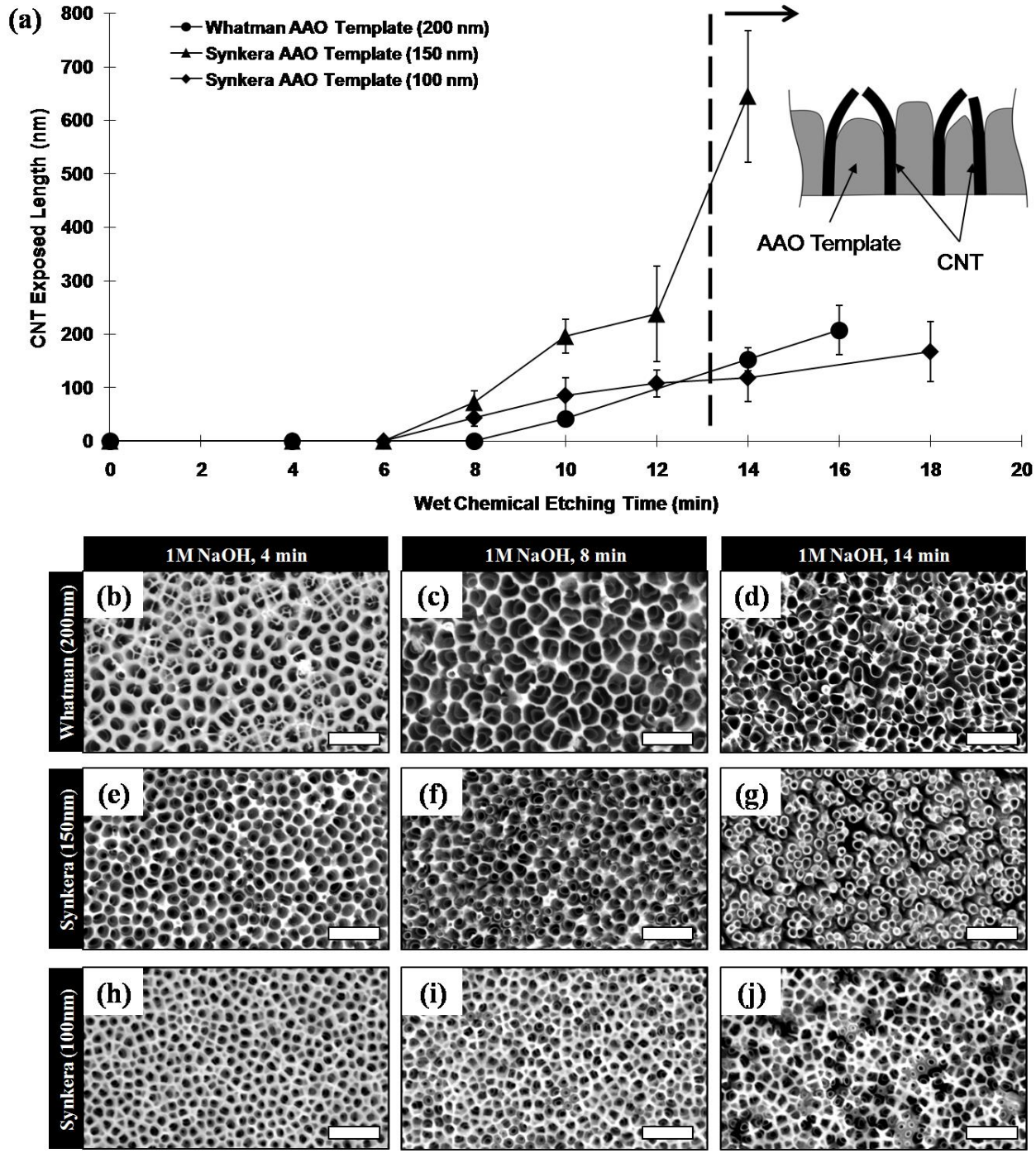

Fig. 7: Effect of wet chemical etching time on CNT exposure. (a) CNT exposed length as a function of etching time in 1 M aqueous NaOH solution at room temperature for Whatman (200 nm pore diameter, solid circle), Synkera (150 nm pore diameter, solid triangle) and Synkera (100 nm pore diameter, solid dimond). Inset: The schematic of the lateral adhesion of CNTs after long wet etching due to pore widening and the loss of support from the etched AAO template. SEM micrographs of CNT embedded AAO membranes after wet chemical etching in 1 M aqueous NaOH solution for (b, e, h) 4, (c, f, i) 8 and (d, g, j) 14 minutes for (b-d) Whatman 200 nm, (e-g) Synkera 150 nm and (h-j) Synkera 100 nm AAO membranes. (Scale bars: 1 μm)

also utilized. The carbon deposited templates were first submerged in 0.5 M aqueous solution of 5 different acids (sulfuric acid (H_2SO_4), hydrochloric acid (HCl), phosphoric acid (H_3PO_4), acetic acid (CH_3COOH), formic acid (HCOOH)) and 2 bases (sodium hydroxide (NaOH) and potassium hydroxide (KOH)) for 15 minutes at room temperature to elucidate proper etchant.

As shown by the SEM micrographs in Fig. 6, the CNT tips are not visible after etching with acids (Fig. 6 (a-e)). However, CNTs are exposed after etching with two bases (Fig. 6(f, g)). This indicates that only NaOH and KOH can etch the AAO templates in this relatively short time window. This is in agreement with the results from other studies [32, 36, 37].

The effect of etching time on CNT tip exposure was studied using 1 M aqueous NaOH solution for all three membranes (Fig. 7(b-j)). As illustrated in Fig. 7(a), increasing the etching time, increases the CNT exposed length. However, the Synkera 150 nm AAO membrane shows a steeper trend compared to the Whatman membrane. Recalling the pore structure for Whatman and Synkera AAO membranes (Fig. 2), to expose the CNT tips using pure wet chemical etching, the Whatman membrane should be submerged in the etchant to first remove the 1 µm deep branch structure. Therefore, it takes longer to expose CNTs from the Whatman AAO membrane compared to Synkera. Moreover, increased variability (standard deviation) at longer etching time indicates less uniform AAO membrane etching due to the isotropic nature of wet etching process.

A comparison between the exposed CNTs after RIE (Fig. 5 (f)) and wet etching with 1 M aqueous NaOH solution (Fig. 7(d, g, j)) indicates that the exposed CNTs are aggregated into bundles after being wet etched for longer than 14 minutes. This is likely due to the widening of the AAO pores during the wet etching step, which reduces the support of the AAO template for the exposed CNTs. Therefore, the nonuniform etching of the AAO templates, the Van der Waals attraction between the CNTs, and the surface tension of the wet solution during evaporation can cause lateral adhesion of the CNTs after exposure (Fig. 7(a-inset)). Similar results have been observed elsewhere [28, 29]. This suggests that to reach longer individually addressable exposed CNTs, dry etching processes like RIE are more promising.

3) Ion Milling and Wet Chemical Etching

To create individually addressable CNTs protruded from the AAO surface, a combination of ion milling and wet etching was followed. Note that there is a branch shaped structure with a depth of around 1 µm on top of the Whatman AAO template (Fig. 2(a-i)) that needs to be removed before CNT exposure. To this end, the surface of carbon deposited AAO templates were first etched away for 2 hours using ion milling and the CNTs were then exposed by wet etching in aqueous NaOH solution. Fig. 8 shows the embedded CNTs after ion milling process, and also after ion milling followed by 9 and 15 minutes of wet etching with 1M aqueous NaOH solution, resulting in exposed CNTs of 100±27 nm and 183±48 nm, respectively. Despite the fact that ion milling removes a layer from the top surface of AAO template and provides a clean surface for wet etching, the surface has a non-planar morphology. Exposing the CNTs with wet etching after ion milling carries the same pore widening problem observed from wet etching alone, which caused the CNTs to lose their support from the template and adhere to each other after a certain point, resulting in less controllability over the length of the exposed CNTs.

IV. Conclusion

Vertically aligned, hollow arrays of CNTs can be produced using a three-step template-based nanomanufacturing process. Carbon was deposited inside the pores of AAO templates using CVD to form CNTs. Three different etching processes were explored to expose the CNT tips by selectively removing the AAO template: RIE using BCl_3 and Cl_2 gases, wet chemical etching and ion milling. The results indicate that in RIE process, adding the chlorine gas to the combination expedites the carbon etch rate compare to AAO, preventing the CNT

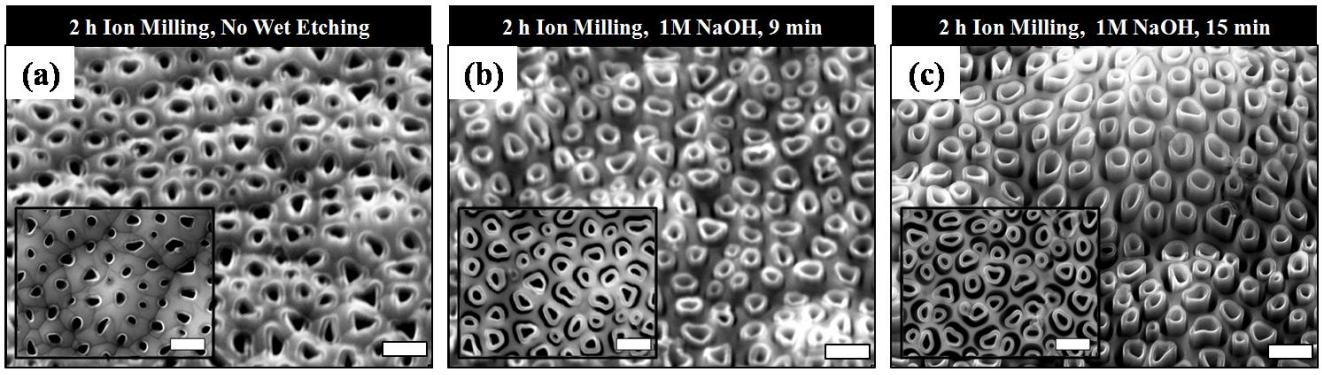

Fig. 8: SEM micrographs (35° tilted view) of CNT embedded Whatman AAO membranes after (a) 2 hours of ion milling, and 2 hours of ion milling followed by (b) 9 minutes and (c) 15 minutes of wet etching using 1 M aqueous NaOH solution at room temperature. Insets: top view SEM micrograph of the same parameter setting. (Scale bars: 500 nm)

exposure. Moreover, increasing the RF power and etching time increase the CNT exposed length. A comparison of several chemical etchants revealed that the two bases, NaOH and KOH, could selectively etch the AAO templates in a relatively short time period. However, creating individually addressable CNTs using only wet etching is challenging due to formation of CNT bundles after etching. This could be due to the loss of support from the AAO templates and Van der Waals attraction forces between CNTs. On the other hand, a combination of ion milling and wet etching served as a hybrid method to expose CNTs but with a non-planar surface morphology. Therefore, the RIE process is a more suitable method to fabricate individually addressable CNTs. The final outcome of this work provides a scalable and reliable manufacturing guideline for a CNT-based array device that can be used for various sensing, biological and biomedical applications.

ACKNOWLDEGEMENT

This work was supported in part by a grant from RIT to establish the American-German Partnership to Advance Biomedical and Energy Applications of Nanocarbon (MGS), the Texas Instruments / Douglas Harvey 2012 RIT Faculty Award (MGS), a grant from the Schmitt Foundation (IMD and MGS), and a grant from the University of Rochester Technology Development Fund (IMD and MGS). MGS was also supported in part by the Feinberg Foundation and Weizmann Institute of Science. The authors are grateful to Richard Hailstone (RIT NanoImaging Laboratory) and Brian McIntyre (University of Rochester Nano Core) for assistance with scanning electron microscopy. The authors also acknowledge the Semiconductors and Microsystems Fabrication Laboratory (SMFL) at Rochester Institute of Technology for RIE machine and technical support.

REFERENCES

[1] M.G. Schrlau, E.M. Falls, B.L. Ziober, and H.H. Bau, “Carbon nanopipettes for cell probes and intracellular injection,” Nanotechnology, 2008. 19(1): p. 015101.

[2] M.G. Schrlau, E. Brailoiu, S. Patel, Y. Gogotsi, N.J. Dun, and H.H. Bau, “Carbon nanopipettes characterize calcium release pathways in breast cancer cells,” Nanotechnology, 2008. 19(32): p. 325102.

[3] K. Yum, N. Wang, and M.-F. Yu, “Nanoneedle: A multifunctional tool for biological studies in living cells,” Nanoscale, 2010. 2(3): p. 363-372.

[4] R. Elnathan, M. Kwiat, F. Patolsky, and N.H. Voelcker, “Engineering vertically aligned semiconductor nanowire arrays for applications in the life sciences,” Nano Today, 2014. 9(2): p. 172-196.

[5] S. Bonde, K.R. Rostgaard, T.K. Andersen, T. Berthing, and K.L. Martinez, “Exploring arrays of vertical one-dimensional nanostructures for cellular investigations,” Nanotechnology, 2014. 25(36): p. 362001.

[6] Y. Alapan, K. Icoz, and U.A. Gurkan, “Micro- and nanodevices integrated with biomolecular probes,” Biotechnology Advances, 2015. 33(8): p. 1727-1743.

[7] K.R. Rostgaard, R.S. Frederiksen, Y.-C.C. Liu, T. Berthing, M.H. Madsen, J. Holm, J. Nygård, and K.L. Martinez, “Vertical nanowire arrays as a versatile platform for protein detection and analysis,” Nanoscale, 2013. 5(21): p. 10226-10235.

[8] V. Krivitsky, L.-C. Hsiung, A. Lichtenstein, B. Brudnik, R. Kantaev, R. Elnathan, A. Pevzner, A. Khatchtourints, and F. Patolsky, “Si nanowires forest-based on-chip biomolecular filtering, separation and preconcentration devices: nanowires do it all,” Nano Letters, 2012. 12(9): p. 4748-4756.

[9] S. Pogodin and V.A. Baulin, “Can a carbon nanotube pierce through a phospholipid bilayer?,” ACS Nano, 2010. 4(9): p. 5293-5300.

[10] T. Berthing, C.B. Sørensen, J. Nygård, and K.L. Martinez, “Applications of nanowire arrays in nanomedicine,” Journal of Nanoneuroscience, 2009. 1(1): p. 3-9.

[11] X. Xie, A.M. Xu, M.R. Angle, N. Tayebi, P. Verma, and N.A. Melosh, “Mechanical model of vertical nanowire cell penetration,” Nano Letters, 2013. 13(12): p. 6002-6008.

[12] Y.-R. Na, S.Y. Kim, J.T. Gaublomme, A.K. Shalek, M. Jorgolli, H. Park, and E.G. Yang, “Probing enzymatic activity inside living cells using a nanowire–cell “sandwich” assay,” Nano Letters, 2012. 13(1): p. 153-158.

[13] A. Hai, J. Shappir, and M.E. Spira, “In-cell recordings by extracellular microelectrodes,” Nature Methods, 2010. 7(3): p. 200-202.

[14] M. Golshadi, L.K. Wright, I.M. Dickerson, and M.G. Schrlau, “High-Efficiency Gene Transfection of Cells through Carbon Nanotube Arrays,” Small, 2016.

[15] A.K. Shalek, J.T. Gaublomme, L. Wang, N. Yosef, N. Chevrier, M.S. Andersen, J.T. Robinson, N. Pochet, D. Neuberg, and R.S. Gertner, “Nanowire-mediated delivery enables functional interrogation of primary immune cells: application to the analysis of chronic lymphocytic leukemia,” Nano Letters, 2012. 12(12): p. 6498-6504.

[16] J.J. Vandersarl, A.M. Xu, and N.A. Melosh, “Nanostraws for direct fluidic intracellular access,” Nano Letters, 2011. 12(8): p. 3881-3886.

[17] S. Park, Y.-S. Kim, W.B. Kim, and S. Jon, “Carbon nanosyringe array as a platform for

intracellular delivery," Nano Letters, 2009. 9(4): p. 1325-1329.

[18] K.S. Brammer, C. Choi, S. Oh, C.J. Cobb, L.S. Connelly, M. Loya, S.D. Kong, and S. Jin, "Antibiofouling, sustained antibiotic release by Si nanowire templates," Nano Letters, 2009. 9(10): p. 3570-3574.

[19] G. Withey, A. Lazareck, M. Tzolov, A. Yin, P. Aich, J. Yeh, and J. Xu, "Ultra-high redox enzyme signal transduction using highly ordered carbon nanotube array electrodes," Biosensors and Bioelectronics, 2006. 21(8): p. 1560-1565.

[20] J. Wang, "Carbon-nanotube based electrochemical biosensors: A review," Electroanalysis, 2005. 17(1): p. 7-14.

[21] M.A. Bucaro, Y. Vasquez, B.D. Hatton, and J. Aizenberg, "Fine-tuning the degree of stem cell polarization and alignment on ordered arrays of high-aspect-ratio nanopillars," ACS Nano, 2012. 6(7): p. 6222-6230.

[22] C.J. Bettinger, R. Langer, and J.T. Borenstein, "Engineering substrate topography at the micro-and nanoscale to control cell function," Angewandte Chemie International Edition, 2009. 48(30): p. 5406-5415.

[23] T. Berthing, S. Bonde, K.R. Rostgaard, M.H. Madsen, C.B. Sørensen, J. Nygård, and K.L. Martinez, "Cell membrane conformation at vertical nanowire array interface revealed by fluorescence imaging," Nanotechnology, 2012. 23(41): p. 415102.

[24] L. Hanson, Z.C. Lin, C. Xie, Y. Cui, and B. Cui, "Characterization of the cell–nanopillar interface by transmission electron microscopy," Nano Letters, 2012. 12(11): p. 5815-5820.

[25] H. Persson, C. Købler, K. Mølhave, L. Samuelson, J.O. Tegenfeldt, S. Oredsson, and C.N. Prinz, "Fibroblasts cultured on nanowires exhibit low motility, impaired cell division, and DNA damage," Small, 2013. 9(23): p. 4006-4016.

[26] M. Golshadi, J. Maita, D. Lanza, M. Zeiger, V. Presser, and M.G. Schrlau, "Effects of synthesis parameters on carbon nanotubes manufactured by template-based chemical vapor deposition," Carbon, 2014. 80: p. 28-39.

[27] W. Lee and S.-J. Park, "Porous anodic aluminum oxide: anodization and templated synthesis of functional nanostructures," Chemical Reviews, 2014. 114(15): p. 7487-7556.

[28] A. Yin, H. Chik, and J. Xu, "Postgrowth processing of carbon nanotube arrays-enabling new functionalities and applications," Nanotechnology, IEEE Transactions on, 2004. 3(1): p. 147-151.

[29] R. Bandyopadhyaya, E. Nativ-Roth, O. Regev, and R. Yerushalmi-Rozen, "Stabilization of individual carbon nanotubes in aqueous solutions," Nano Letters, 2002. 2(1): p. 25-28.

[30] X. Yang, D.-P. Kim, D.-S. Um, G.-H. Kim, and C.-I. Kim, "Temperature dependence on dry etching of Al2O3 thin films in BCl3/Cl2/Ar plasma," Journal of Vacuum Science & Technology A, 2009. 27(4): p. 821-825.

[31] X. Yang, J.-C. Woo, D.-S. Um, and C.-I. Kim, "Dry Etching of Al 2 O 3 Thin Films in O 2/BCl 3/Ar Inductively Coupled Plasma," Transactions on Electrical and Electronic Materials, 2010. 11(5): p. 202-205.

[32] K.R. Williams, K. Gupta, and M. Wasilik, "Etch rates for micromachining processing-Part II," Microelectromechanical Systems, Journal of, 2003. 12(6): p. 761-778.

[33] J. Yeon, W. Lim, J. Park, N. Kwon, S. Kim, K. Min, I. Chung, Y. Kim, and G. Yeom, "Removal of Anodic Aluminum Oxide Barrier Layer on Silicon Substrate by using Cl2/BCl3 Neutral Beam Etching," Journal of the Electrochemical Society, 2011. 158(5): p. D254-D258.

[34] X. Yang and D.S. Um, "Regular Paper: Dry Etching of Al2O3 Thin Films in O2/BCl3/Ar Inductively Coupled Plasma," Trans. Electr. Electron. Mater.(TEEM), 2010. 11(5): p. 202-205.

[35] K. Tokunaga, F. Redeker, D. Danner, and D. Hess, "Comparison of aluminum etch rates in carbon tetrachloride and boron trichloride plasmas," Journal of the Electrochemical Society, 1981. 128(4): p. 851-855.

[36] M. Golshadi and M.G. Schrlau, "Template-based synthesis of aligned carbon nanotube arrays for microfluidic and nanofluidic applications," ECS Transactions, 2013. 50(33): p. 1-14.

[37] K.R. Williams and R.S. Muller, "Etch rates for micromachining processing," Microelectromechanical Systems, Journal of, 1996. 5(4): p. 256-269.